A Packing Model for Interpenetrated Diamondoid Structures—An Interpretation Based on the Constructive Interference of Supramolecular Networks

Keith A. Hirsch, Scott R. Wilson, and Jeffrey S. Moore*

Abstract: The ability to predict and subsequently control solid-state structure has been identified as a major challenge in the field of crystal engineering. Here we suggest the concept of constitutive models as a tool for understanding crystal packings and for designing new solid-state structures. Such models are intended to relate molecular interactions and their geometrical constraints with solid-state organization. These models will most likely be of greatest use for crystals consisting of supramolecular networks, that is, infinite assemblies of small molecules associating through strong, directional, and selective noncovalent interactions. The concept of the constitutive packing model is illustrated for interpenetrated diamondoid coordination networks based on crystalline adducts of 4,4′-biphenyldicarbonitrile with silver(I) salts. Observed structural deformations induced by counterions of varying size may be understood in terms of the interference of two supramolecular networks within this system: the diamondoid metal–ligand coordination network and face-to-face aromatic stacks of the organic ligand. The constitutive model developed here has been applied to other diamondoid coordination networks in the literature and is found to be general.

Keywords
aromatic stacking · crystal engineering · diamondoid networks · packing model · supramolecular chemistry

Introduction

The field of crystal engineering has evolved from the pioneering ideas of Schmidt[1] into one of intense interest due to the widely held belief that the ability to control molecular organization in the solid state will lead to materials of novel structure and function.[2] However, the prediction of solid-state packing remains a difficult challenge due to the delicate competition among the many noncovalent interactions which enter into the crystal field. To address this problem, we present a new tool to aid in the conception of reasonable starting points for solid-state structures—the constitutive model of crystal packing. A constitutive packing model originates from the analysis of a series of related crystal structures with focus on the dominant supramolecular networks. The ultimate goal of predicting crystal structures, given the myriad of potential packings, will require the development of collections of such models for the many possible network topologies.[3] For a given compound, the feasibility of attaining a particular solid-state structure may be determined by considering each of the plausible packings relative to other models. Once candidate structures have been identified, energy minimization could then be used to pinpoint the structure most likely to form.

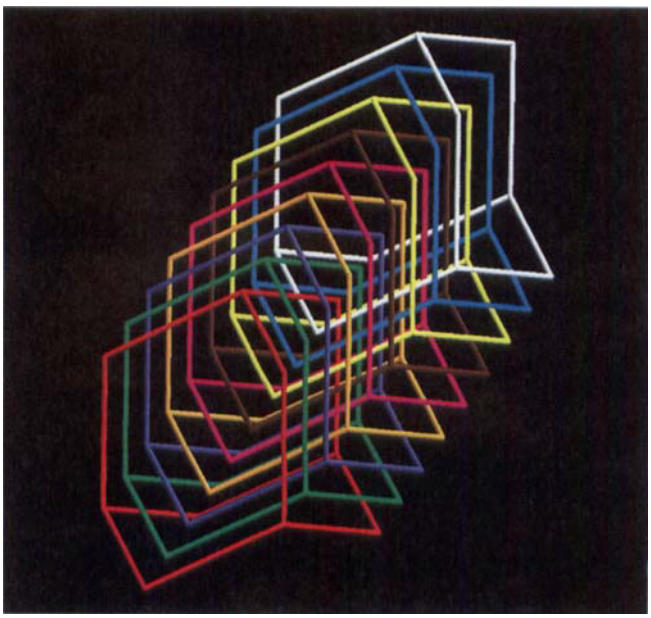

Figure 1. Nine interpenetrated adamantanoid cages created from the diamondoid crystal structure of BPCN with $AgPF_6$ from ethanol (disordered counterions have been removed for clarity). Tetrahedral silver(I) ions are located at the vertices, and bridging molecules of BPCN have been replaced with cylinders for simplicity.

[*] Prof. J. S. Moore, Dr. S. R. Wilson, K. A. Hirsch
Departments of Chemistry and Materials Science and Engineering
The University of Illinois at Urbana-Champaign
Box 55-5, 600 S. Mathews Ave., Urbana, IL 61801 (USA)
Fax: Int. code +(217)244-8068
e-mail: moore@aries.scs.uiuc.edu

  0947-6539/97/0305-0765 $ 17.50+.50/0

Herein, we develop a constitutive packing model for interpenetrated diamondoid networks.[4] The model is based on ninefold diamondoid structures of 4,4′-biphenyldicarbonitrile (BPCN) with $AgPF_6$, $AgAsF_6$, or $AgSbF_6$. We believe that the development of packing models such as this is an important first step in the accurate prediction and subsequent design of molecular crystals.

Results and Discussion

Diamondoid network deformation as a function of counterion size: Previously, we reported that complexation of BPCN with $AgPF_6$ in ethanol yields a crystalline diamondoid network formed by coordination of BPCN ligands to tetrahedral silver(I) ions.[4a, b] The network is relatively undistorted in comparison to diamond, as N-Ag-N bond angles range from 108.9 to 110.6°. The large amount of void space present in a single diamondoid network is filled primarily by the interpenetration of eight other identical networks (ninefold interpenetration). Despite this high level of interpenetration, channels along the *c* axis are maintained, which are occupied by disordered PF_6^- ions. Interpenetration in this structure may be viewed in terms of the concatenation of nine adamantanoid cages as shown schematically in Figure 1.

An alternative manner in which the packing of the diamondoid network may be understood is to consider a structural subunit of an adamantanoid cage, the 4/1 helix shown in Figure 2a.[4l, m] The value of depicting the structure this way becomes evident from the simplification it provides to the complex picture of nine interwoven 3-D networks. Rather than viewing the ninefold interpenetration in terms of adamantanoid cages, the packing may be described as the intertwining of nine 4/1 helices, which form the walls of the counterion channels (Figure 2b).[5] This dichotomy clearly illustrates the subjective nature of crystal structure interpretation. It is evident from Figure 2b that molecules of BPCN interact through face-to-face π–π stacking. In particular, a plane-to-plane distance of 3.60 Å and an offset angle of 42.0° are observed. Figure 2c shows that the helix pitch is spanned by a π-stack of BPCN molecules, one ligand from each of the nine independent networks. There is

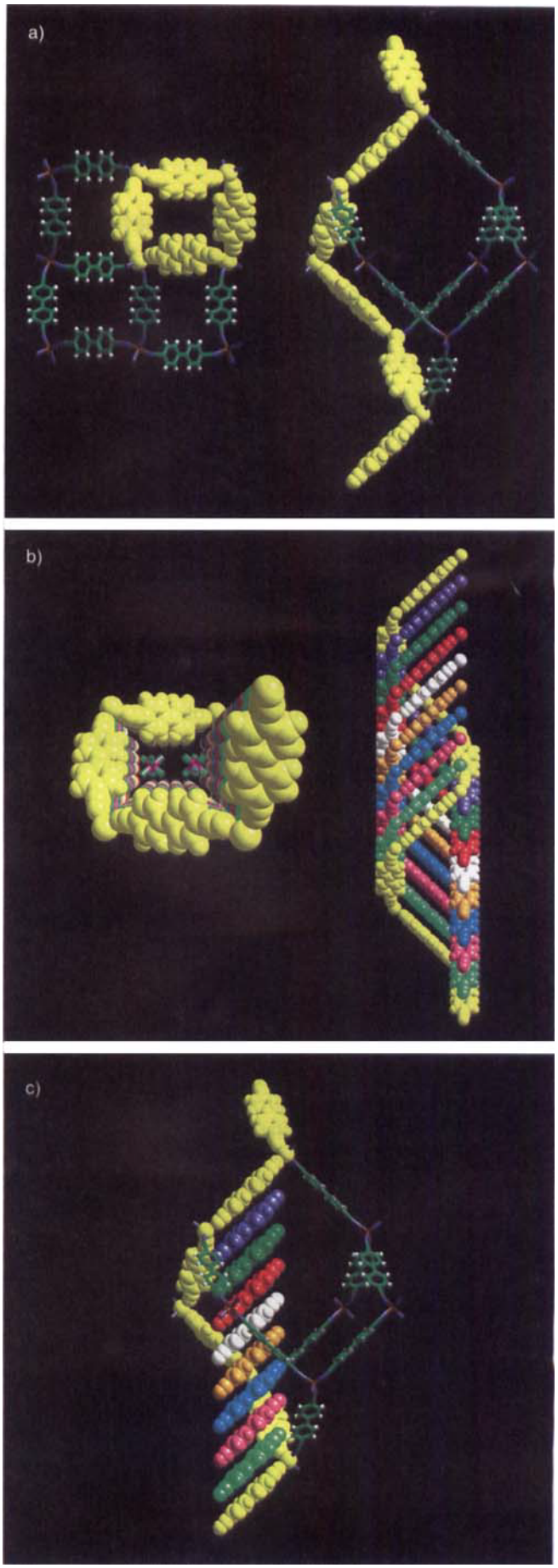

Figure 2. Interpretation of the packing of the ninefold interpenetrated diamondoid network of BPCN and $AgPF_6$ in terms of the 4/1 helix. a) The 4/1 helix as a structural subunit of an adamantanoid cage. Left: view along the helix axis, which is also the counterion channel axis (disordered PF_6^- ions have been omitted for clarity). The 4/1 helix forms the boundary of a counterion channel. Right: view perpendicular to the counterion channel/helix axis reveals how the helix is related to the adamantanoid cage. The helix pitch is the length of the body diagonal of the cage. b) The nine intertwined helices that form the walls of the counterion channel. This arrangement arises from the interpenetration of nine diamondoid networks (note that each helix, indicated by a different color, originates from an independent network). Left: perspective view along the counterion channel/helix axis with disordered PF_6^- ions (fluorine is green and phosphorous is magenta). Right: view perpendicular to the counterion channel/helix axis. Note that the walls of the counterion channel are formed from four separate π-stacks of BPCN; π–π stacking of BPCN occurs at a plane-to-plane distance of 3.60 Å with an offset angle of 42.0°. c) The 4/1 helix in an adamantanoid cage showing the perfect coincidence between helix pitch and the stack of nine BPCN ligands.

0947-6539/97/0305-0766 $ 17.50+.50/0 Chem. Eur. J. 1997, 3, No. 5

clearly perfect metric match between the pitch of the helix and the height of an offset stack of nine BPCN ligands.

The interpretative value of structural deformations induced by the incorporation of different size guests was recognized early on by Powell in the context of clathrates of quinol with small guest inclusions.[6] Other early reports illustrating the effect of composition on structure have been summarized by Hazen and Finger.[7] In this same vein, we studied the changes induced in the BPCN diamondoid structure for counterions of varying size. Crystallization of BPCN with $AgSbF_6$ from ethanol results in the formation of a diamondoid network of similar topology (complex **1**). As with the $AgPF_6$ structure, the network is ninefold interpenetrated through face-to-face stacking of BPCN at a plane-to-plane distance of 3.59 Å. However, the structure is significantly distorted, as N-Ag-N bond angles range from 95.4 to 118.4°. The consequence of these local deformations is that the helix pitch is elongated by approximately 18% relative to that in the $AgPF_6$ structure (43.61 Å for $AgPF_6$ vs. 51.32 Å for $AgSbF_6$). This stretching alters the offset angle of the π-stack from 42.0° with $AgPF_6$ to 51.0° in the $AgSbF_6$ adduct (Figure 3). Considering interpenetration, an equivalent stretching of all nine helices comprising the counterion channel takes place. This elongation leads to lateral compressions which alter the shape of the counterion channel (Figure 3). The deformation probably occurs in order to efficiently accommodate the larger SbF_6^- ion,[8] as it increases the anion–anion separation along the channel axis. Specifically, the anion–anion separation is 4.85 Å for the $AgPF_6$ structure as compared to 5.70 Å for the $AgSbF_6$ example. The $AgSbF_6$ structure exhibits slight counterion disorder over two sites along the channel axis. The major site occupancy is 0.93.

Crystallization of BPCN with $AgAsF_6$ from ethanol was also examined. This experiment employed the AsF_6^- ion, which is intermediate in size for the series studied ($PF_6^- < AsF_6^- < SbF_6^-$).[8] In this case, two polymorphs are obtained. Both of these polymorphs are ninefold interpenetrated diamondoid networks. The first, polymorph I (complex **2**), is similar to the $AgPF_6$ structure, as N-Ag-N bond angles range from 108.8 to 110.8°. The shape of the counterion channel in polymorph I is also similar to that for $AgPF_6$. However, the helix pitch (43.21 Å) and offset angle (41.8°) are slightly less (Figure 3). The subtle decrease in the helix pitch and offset angle observed with $AgAsF_6$ allows lateral expansion of the counterion channel to accommodate the larger AsF_6^- ion. The AsF_6^- ions are disordered over two sites in a mode comparable to that observed with $AgPF_6$ (Figure 2b).

Polymorph II (complex **3**) structurally resembles the $AgSbF_6$ structure, as demonstrated by the N-Ag-N bond angles ranging from 94.1 to 118.0°. The shape of the counterion channel for polymorph II is also similar to that observed for the $AgSbF_6$ example. However, the helix pitch (51.94 Å) and offset angle (51.8°) are slightly greater for polymorph II (Figure 3). These small increases relative to the BPCN·$AgSbF_6$ adduct can be understood as a lateral compression of the counterion channel to better accommodate the smaller AsF_6^- ion. The AsF_6^- ions in this structure are significantly disordered along the channel axis.

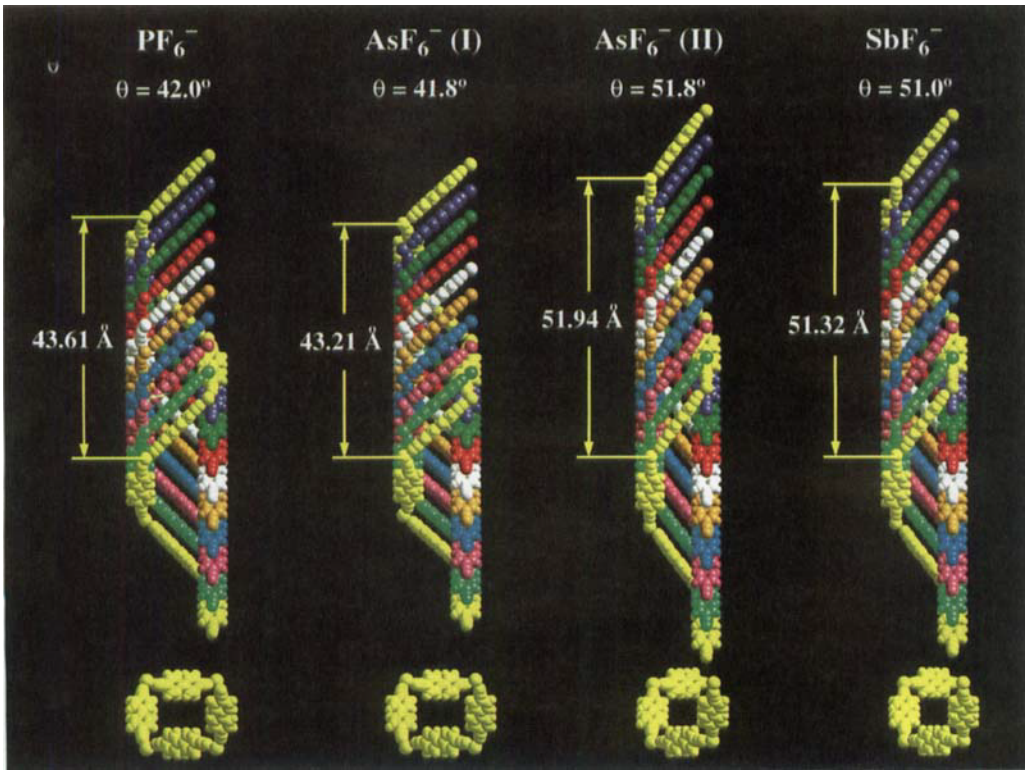

Figure 3. Counterion channels formed from the intertwining of 4/1 helices for diamondoid networks obtained with BPCN and $AgPF_6$, $AgAsF_6$, and $AgSbF_6$. The helix pitch and offset angles are labeled. A view along the counterion channel/helix axis is shown for each example. Two polymorphs are obtained with $AgAsF_6$. A deformation of the diamondoid network concomitant with a change in the offset angle of π–π stacking is observed upon counterion substitution. These deformations, therefore, arise through constructive interference between two supramolecular networks in these structures. It should be noted that with the AsF_6^- ion, which is intermediate in size for this series, a diamondoid network with intermediate values for the helix pitch and offset angle does not form.

It is interesting that the AsF_6^- ion is accommodated in diamondoid networks similar to those described for both $AgPF_6$ and $AgSbF_6$. Thus, the counterion of intermediate size does not cause the diamondoid network to deform to an intermediate helix pitch and offset angle. It is possible that the two general types of diamondoid networks observed represent two optimal π-stacked arrangements of the BPCN ligand within this framework.

A constitutive packing model for interpenetrated diamondoid structures: In considering Figure 2c one can perceive two supramolecular networks, each with its own characteristic repeating period. The first network is the diamondoid coordination

network with the period defined by the helix pitch. The second is the one-dimensional π-stack of BPCN whose period is defined by the van der Waals thickness of the aromatic ring. The two periods are independent, since the helix pitch is a function of the ligand length and offset angle, while the π-stack repeat is $s/\cos\theta$, where s is the face-to-face stacking distance and θ is the offset angle (Figure 4). The two networks are directionally coincident

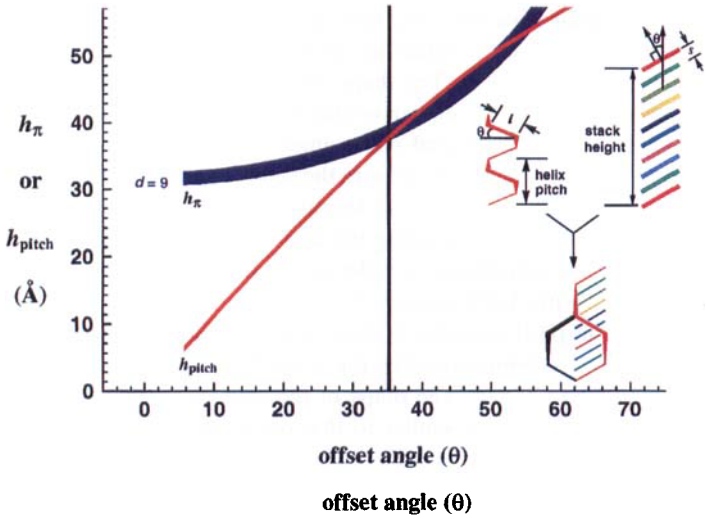

offset angle (θ)

Figure 4. A constitutive packing model for diamondoid networks: The red curve, representing the helix pitch (h_{pitch}), is shown for a value of l of 16.4 Å, which corresponds to the Ag–BPCN–Ag distance in the diamondoid structure of BPCN and $AgPF_6$. The blue curve, representing the stack height (h_π), is shown for a degree of interpenetration (d) of 9. A band has been plotted since values of the π–π stacking distances of 3.4 and 3.6 Å have been considered. The region in which the red curve overlaps the blue band (i.e., where $h_{pitch} = h_\pi$) represents reasonable combinations of the helix pitch and offset angle for a diamondoid network with a ninefold degree of interpenetration. The wide region of overlap for $d = 9$ is particularly noteworthy. The model implies that the ninefold diamondoid network is capable of undergoing significant deformation. The schematics on the right illustrate π–π stacking mediated interpenetration for the diamondoid network that is brought about by the coincidence of h_{pitch} and h_π. Key packing parameters are defined in terms of the 4/1 helix and a π-stack of aromatic rings, as indicated. The black vertical line at $\theta = 35.25°$ represents the offset angle of a diamondoid network with perfect tetrahedral valence angles.

and coupled through θ; therefore, they may spatially interfere with one another, and this interference can be modulated by θ.[9] This implies that a deformation of the diamondoid network, which may be realized through compression and expansion of bond angles about the metal ion, should be accompanied by a concomitant deformation in the π–π stacking of BPCN through variation of the offset angle of stacking. The ideal offset angle is 35.25° if the tetrahedral valence angle in diamond of 109.5° is considered. A simple relation between the helix pitch (h_{pitch}) and the offset angle (θ) is given by Equation (1), where l is the metal–ligand–metal separation (Figure 2a).

$$h_{pitch} = 4l(\sin\theta) \quad (1)$$

As illustrated in Figure 2c, interpenetration of the diamondoid network is mediated by face-to-face π–π stacking of BPCN within the space defined as the helix pitch. Therefore, the degree of interpenetration (d) may be defined as the number of ligands from individual networks π-stacked within the repeat period of the diamondoid network. The height of a π-stack (h_π) having d interlayer spaces and tilted with offset θ is given by Equation (2), where s is the fixed value of the perpendicular,

$$h_\pi = \frac{ds}{\cos\theta} \quad (2)$$

plane-to-plane stacking distance of aromatic ligands. Integer values of d and the corresponding values of θ that bring about coincidence between h_{pitch} and h_π define the plausible packings for this model. This can be clearly understood with a graphical explanation. Shown in Figure 4 is an overlay of plots constructed from Equations (1) and (2). Helix pitch (red curve) has been plotted for the value of l corresponding to the metal–ligand–metal separation observed in the diamondoid network formed from BPCN and $AgPF_6$ (ca. 16.4 Å). The blue curve represents the height of a stack of nine BPCN ligands ($d = 9$). This curve has been constructed for values of s in the range of 3.4 to 3.6 Å since they represent one standard deviation about the mean of 3.5 Å observed for all stacked aromatics in the Cambridge Structural Database.[10] Thus, a band results wherein the lower regime represents solutions for a stacking distance of 3.4 Å and the upper regime represents solutions for a stacking distance of 3.6 Å. It is important to note that points of overlap of the red curve with the blue band represent the offset angles that can, in principle, lead to a diamondoid network of $d = 9$ and $l = 16.4$ Å. In other words, the points of intersection represent reasonable packings. It is noted that for the value of l equal to the Ag–BPCN–Ag distance, a large region of overlap is observed for a degree of interpenetration of nine (Figure 4). The model implies that the ninefold interpenetrated diamondoid system can simultaneously meet the distance requirements of π–π stacking and helix pitch over a range of offset angles. For the diamondoid networks presented here, deformations over this range were observed experimentally by counterion substitution (Figure 3).

The constitutive model may also be applied to the packing of counterions within channels formed by the diamondoid framework. The counterions in this study can be approximated as spheres with diameters of 4.68, 4.94, and 5.14 Å for PF_6^-, AsF_6^-, and SbF_6^-, respectively. These diameters were calculated from published counterion volumes.[8] Charge balance considerations and the closest packing of spheres along the counterion channel axis suggest a commensurate, periodic repeat of d times the counterion diameter, where d is the degree of interpenetration. Shown in Figure 5 is an overlay plot similar to that shown in Figure 4. Degrees of interpenetration of 8–10 are now considered. The red curve is plotted for $l = 16.4$ Å, as in Figure 4. The horizontal arrows represent d times the counterion diameter for the PF_6^-, AsF_6^-, and SbF_6^- ions. For clarity, only one data point is shown in Figure 5 for $d = 8$ and 10, although all three are shown for $d = 9$. The plot shows that the dark blue arrows (the repeat distances for stacks of nine anions) intersect the red curve in the region of $d = 9$ (no other value of d is considered, owing to the requirement of charge neutrality). This illustrates that a ninefold diamondoid network with $l = 16.4$ Å is plausible with inclusion of any of these anions. Further, the light blue arrow (the repeat distance of eight PF_6^- ions) does not coincide with the red curve in the region of $d = 8$. Similarly, the magenta arrow (the repeat distance of ten SbF_6^- ions) does not coincide with the red curve for $d = 10$. Thus, the plot shows that eight- and tenfold interpenetration is not feasible with BPCN

0947-6539/97/0305-0768 $ 17.50+.50/0 Chem. Eur. J. 1997, 3, No. 5

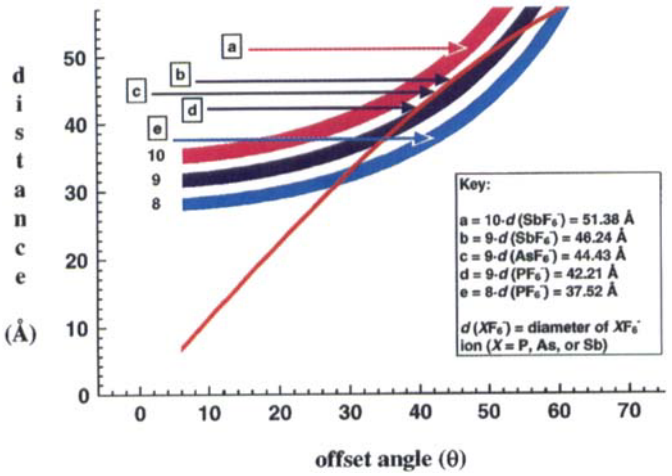

Figure 5. A constitutive model for diamondoid networks in terms of the packing of counterions. Counterions are considered to pack as spheres along the channel axis. The number of anions that span the helix pitch defines the degree of interpenetration due to the requirement of charge neutrality. For this plot, degrees of interpenetration of 8–10 are considered, and the red curve is shown for $l = 16.4$ Å. The horizontal arrows represent the degree of interpenetration times the anion diameter, as indicated in the key. Counterion diameters have been calculated from published volumes (ref. [8]). The dark blue arrows (nine times the anion diameter) intersect the red curve in the region of ninefold interpenetration. This illustrates that a ninefold interpenetrated diamondoid network with $l = 16.4$ Å is consistent with incorporation of either the PF_6^-, AsF_6^-, or SbF_6^- ions. The light blue arrow (eight times the diameter of the PF_6^- ion) does not coincide with the red curve in the region of an eightfold interpenetrated structure. Similarly, the magenta arrow (ten times the diameter of the SbF_6^- ion) does not intersect the red curve for a tenfold structure. Therefore, the plot shows that eight- and tenfold interpenetrated diamondoid networks with $l = 16.4$ Å are not consistent with inclusion of these anions. Similar analysis showed that for all three anions, and $d = 8–10$, $d = 9$ is the only reasonable packing.

($l = 16.4$ Å) and these anions. The practical value of this analysis is that for a given ligand (and, therefore, for a given value of l), diamondoid networks of a particular degree of interpenetration may be targeted and the appropriate counterion size may be selected.

In order to generalize the constitutive model to other ligands, we can construct a map of plausible packings by setting $h_{pitch} = h_\pi$ [Eqs. (1) and (2)], which leads to Equation (3). This equation

$$l = \frac{ds}{2(\sin 2\theta)} \qquad (3)$$

suggests that the only essential molecular variable of this model is l, which, upon subtraction of the metal–ligand bond distances, gives the length of the ditopic ligand. Shown in Figure 6 is a plot of the metal–ligand–metal separation (l) versus the offset angle (θ). The plot has been constructed for degrees of interpenetration (d) of 1–9. For each degree of interpenetration, a band results, as stacking distances (s) of 3.4 and 3.6 Å were used. A horizontal line of fixed l intersects curves that represent various degrees of interpenetration at the indicated offset angles. The combinations of l and θ observed for the diamondoid networks of BPCN and $AgPF_6$, $AgAsF_6$, and $AgSbF_6$ have been identified in Figure 6 and these combinations are found to fall within the region corresponding to ninefold interpenetration.

Two examples of interpenetrated diamondoid networks from the literature have also been analyzed by our model to further test its utility. To our knowledge, these constitute the only examples of diamondoid networks other than those involving BPCN in which interpenetration is mediated by face-to-face stacking of coordinated ligands. The first example is the sevenfold interpenetrated diamondoid networks of the radical anion salts of substituted dicyanoquinonediimines and copper reported by Ermer[4d] and Hünig et al.[4m] For this series of structures, a value of l of approximately 12.7 Å along with an offset angle of 33.0° is observed. This combination of l and θ is plotted in Figure 6 (orange arrow). It is noted that this data point lies below the curve corresponding to a degree of interpenetration of seven. However, these structures feature a rather short π–π stacking distance of only 3.15 Å,[4d] which falls outside the range used to construct Figure 6 (3.4–3.6 Å). Thus, if the curve for $d = 7$ were constructed with a value of s of 3.15 Å, the combination of l and θ observed for this system would lie on this curve.

A second example from the literature that has been applied to the model is the distorted fourfold diamondoid network of 4-cyanopyridine and $AgBF_4$ reported by Ciani et al.[4i] For this structure, a value of l of approximately 9.9 Å and an offset angle of 30.5° is noted. This combination of l and θ is also included in Figure 6 (purple arrow). In this case, the data point lies above

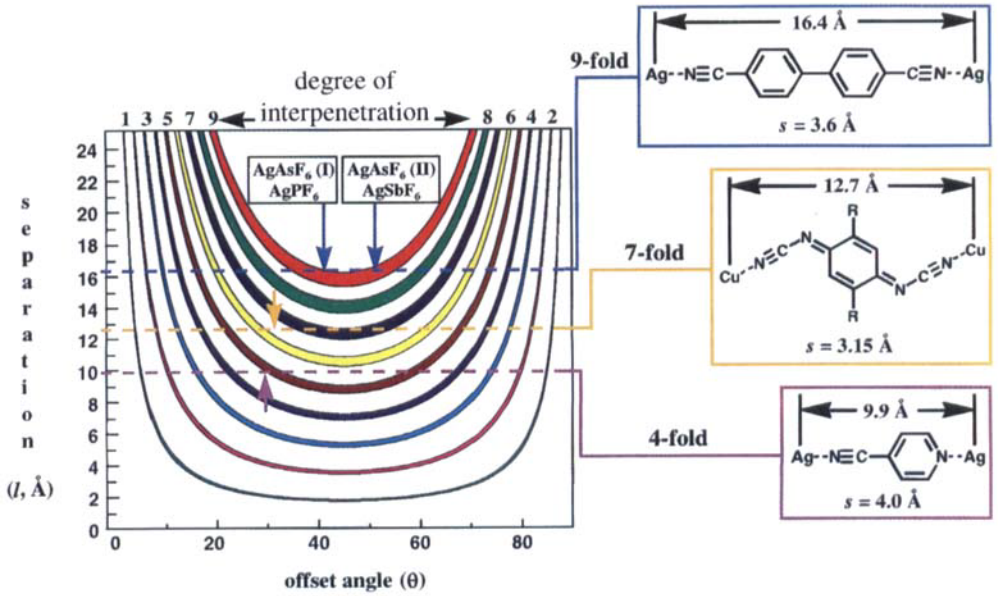

Figure 6. A map of plausible packings for interpenetrated diamondoid networks constructed using Equation (3). Degrees of interpenetration (d) of 1–9 are represented. Colored bands result as π–π stacking distances of 3.4 and 3.6 Å have been considered. The combinations of l and θ observed in the diamondoid structures of BPCN and silver(I) salts are included. Also plotted, are points corresponding to diamondoid structures previously reported in the literature. For the structures of substituted dicyanoquinonediimines and copper ($d = 7$), reported by Ermer (ref. [4d]) and Hünig et al. (ref. [4m]), the observed data point (orange arrow) lies below the curve for $d = 7$, owing to the short stacking distance of 3.15 Å. For the distorted structure of 4-cyanopyridine and $AgBF_4$ ($d = 4$) reported by Ciani et al. (ref. [4i]), the observed data point (purple arrow) lies above the curve for $d = 4$, owing to the long stacking distance of 4.0 Å. If the range of stacking distances were widened to include these unusual values, the model would approximate the observed degrees of interpenetration.

the curve for a degree of interpenetration of four. The reason is that the observed stacking distance is approximately 4.0 Å, which is very long for $\pi-\pi$ stacking and is outside the range used to generate Figure 6. Therefore, if the curve for $d = 4$ were plotted for a value of s of 4.0 Å, this combination of l and θ would approximate the observed degree of interpenetration. It should be emphasized that values of s of 3.4 and 3.6 Å were chosen to construct Figure 6, since they are within a standard deviation of the average $\pi-\pi$ stacking distance in the Cambridge Structural Database of 3.5 Å[10] (this narrow range was further chosen for clarity as bands in the plot would overlap otherwise). Thus, despite the variance observed in the face-to-face stacking distance in these diamondoid networks, the constitutive model presented is found to be applicable beyond the original system for which it was developed.

Conclusion

In summary, we generalize a set of guidelines that can be used to formulate constitutive packing models:

1) Identify the most significant supramolecular networks (two or more).
2) Consider constructive interference between them (i.e., consider networks that are directionally coincident).
3) Identify a compliant deformation process that modulates this interference.

We believe that the development of constitutive packing models for other topologies through the recognition of interfering supramolecular networks will be an important step in being able to predict structure a priori. In due course, collections of these constitutive models will be available to offer reasonable choices of possible packings for the crystal engineer.

Experimental Section

4,4′-biphenyldicarbonitrile (BPCN) was prepared from 4,4′-dibromobiphenyl by a known literature procedure for the conversion of aryl bromides to benzonitriles.[11] $AgAsF_6$ and $AgSbF_6$ were stored in a desiccator before use. X-ray data were collected on a Siemens SMART system with a CCD detector at −75 °C with $Mo_{K\alpha}$ ($\lambda = 0.71073$ Å) as the incident radiation. The intensity data were reduced by profile analysis and corrected for Lorentz, polarization, and absorption effects.

$[Ag(BPCN)_2]SbF_6$ (**1**): A mixture of BPCN (10 mg, 0.05 mmol) and $AgSbF_6$ (19 mg, 0.05 mmol) in absolute ethanol (4 mL) was prepared in a clean vial with a Teflon-lined screw cap. The mixture was heated in an oil bath to 98 °C over 80 min, at which point a homogeneous solution resulted. Cooling to room temperature overnight yielded complex **1** as yellow plates. X-ray data collection was accomplished with a crystal with approximate dimensions of $0.76 \times 0.05 \times 0.05$ mm. Accurate cell dimensions were obtained from the setting angles of 3055 reflections with $5 \le \theta \le 23°$. Crystal data: $C_{28}H_{16}N_4F_6AgSb$; $M_r = 752.07$; space group: triclinic, $I-1$ (no. 2); $a = 5.702(1)$, $b = 21.661(2)$, $c = 21.569(2)$ Å, $\alpha = 89.98(1)°$, $\beta = 89.99(1)°$, $\gamma = 89.99(1)°$; $V = 2663.90(12)$ Å^3; $Z = 4$; $\rho_{calcd} = 1.875$ g cm^{-3}; $2\theta_{max} = 46°$; scan mode: ω scans; $F(000) = 1456$; number of reflections measured = 5224; number of independent reflections = 3716; number of reflections refined = 3716; σ limit: $2\sigma(I)$; absorption correction: integration, $T_{min} = 0.80$, $T_{max} = 0.92$, $\mu(Mo_{K\alpha}) = 1.817$ mm^{-1}; structure solution: direct methods, structure refinement: least-squares against F_o^2 using SHELXTL; number of parameters = 380; hydrogen atoms were included as fixed contributors in idealized positions; $R1 = \sum(|F_o| - |F_c|)/\sum|F_o| = 0.0429$ ($3458 F_o > 4\sigma$), 0.0492 (all data); $wR2 = [\sum(w|F_o^2 - F_c^2|)/\sum w|F_o^2|^2]^{1/2} = 0.1051$ (all data); $S = [\sum w(F_o^2 - F_c^2)^2/(N-P)]^{1/2} = 1.132$ (all data); highest peak in final difference map = + 0.62 e$^-$ Å^{-3}. The alternate space group was chosen to facilitate refinement in body-centered tetragonal space groups. Framework disorder was noted for all tetragonal models. The proposed structural model in $I-1$ includes tetragonal twinning. Occupancies for the four metrically superimposable twin components converged at 0.331(2), 0.169(2), 0.268(2), and 0.232(2).

$[Ag(BPCN)_2]AsF_6$ (**2** and **3**): A mixture of BPCN (10 mg, 0.05 mmol) and $AgAsF_6$ (16 mg, 0.05 mmol) in absolute ethanol (4 mL) was prepared in a clean vial with a Teflon-lined screw cap. The mixture was heated in an oil bath to 104 °C over 64 min, at which point a homogeneous solution resulted. Cooling to room temperature overnight yielded two polymorphs: complex **2** as thin yellow needles and complex **3** as thin yellow plates. Both polymorphs were characterized by X-ray diffraction. For complex **2**, X-ray data collection was accomplished with a crystal with approximate dimensions of $0.02 \times 0.02 \times 0.8$ mm. Accurate cell dimensions were obtained from the setting angles of 2007 reflections with $5 \le \theta \le 23°$. Crystal data for complex **2**: $C_{28}H_{16}N_4F_6AsAg$; $M_r = 705.24$; space group: tetragonal, $I-42d$ (no. 122); $a = b = 24.861(2)$, $c = 4.802(2)$ Å, $\alpha = \beta = \gamma = 90°$; $V = 2967.63(15)$ Å^3; $Z = 4$; $\rho_{calcd} = 1.578$ g cm^{-3}; $2\theta_{max} = 46°$; scan mode: ω scans; $F(000) = 1384$; number of reflections measured = 5673; number of independent reflections = 1078; number of reflections refined = 1078; σ limit: $2\sigma(I)$; absorption correction: empirical, $T_{min} = 0.77$, $T_{max} = 0.99$, $\mu(Mo_{K\alpha}) = 1.847$ mm^{-1}; structure solution: direct methods, structure refinement: least-squares against F_o^2 using SHELXTL; number of parameters = 138; hydrogen atoms were included as fixed contributors in idealized positions; $R1 = 0.0489$ ($949 F_o > 4\sigma$), 0.0591 (all data); $wR2 = 0.1465$ (all data); $S = 1.193$ (all data); highest peak in final difference map = + 0.67 e$^-$ Å^{-3}. For complex **3**, X-ray data collection was accomplished with a crystal of approximate dimensions of $0.4 \times 0.2 \times 0.2$ mm. Accurate cell dimensions were obtained from the setting angles of 1640 reflections with $5 \le \theta \le 28°$. Crystal data for complex **3**: $C_{28}H_{16}N_4F_6AsAg$; $M_r = 705.24$; space group: orthorhombic, $Fddd$ (no. 70); $a = 5.772(1)$, $b = 29.452(2)$, $c = 30.512(2)$ Å, $\alpha = \beta = \gamma = 90°$; $V = 5186.5(3)$ Å^3; $Z = 8$; $\rho_{calcd} = 1.806$ g cm^{-3}; $2\theta_{max} = 56°$; scan mode: ω scans; $F(000) = 2768$; number of reflections measured = 7531; number of independent reflections = 1598; number of reflections refined = 1598; σ limit: $2\sigma(I)$; absorption correction: integration, $T_{min} = 0.55$, $T_{max} = 0.96$, $\mu(Mo_{K\alpha}) = 2.113$ mm^{-1}; structure solution: direct methods, structure refinement: least-squares against F_o^2 using SHELXTL; number of parameters = 204; hydrogen atoms were included as fixed contributors in idealized positions; $R1 = 0.0748$ ($1060 F_o > 4\sigma$), 0.1184 (all data); $wR2 = 0.2224$ (all data); $S = 1.199$ (all data); highest peak in final difference map = + 1.09 e$^-$ Å^{-3}.

Crystallographic data (excluding structure factors) for the structures reported in this paper have been deposited with the Cambridge Crystallographic Data Centre as supplementary publication no. CCDC-100146. Copies of the data can be obtained free of charge on application to The Director, CCDC, 12 Union Road, Cambridge CB21EZ, UK (Fax: Int. code +(1223)336-033; e-mail: deposit@chemcrys.cam.ac.uk).

Acknowledgments: We thank the School of Chemical Sciences Materials Chemistry Laboratory at the University of Illinois for X-ray data collection. We acknowledge the US National Science Foundation (Grant CHE-94-23121) and the US Department of Energy through the Materials Research Laboratory at the University of Illinois at Urbana-Champaign (Grant DE-FG02-91-ER45439) for financial support of this work. Additional support from the Camille Dreyfus Teacher-Scholar Awards Program is gratefully acknowledged. We also thank Professor Stephen Lee at The University of Michigan for many helpful discussions.

Received: December 23, 1996 [F 562]

[1] G. M. J. Schmidt, *Pure Appl. Chem.* **1971**, *27*, 647–678.
[2] a) G. R. Desiraju, *Crystal Engineering: The Design of Organic Solids*, Elsevier, New York, **1989**; b) G. R. Desiraju, *Angew. Chem.* **1995**, *107*, 2541–2558; *Angew. Chem. Int. Ed. Engl.* **1995**, *34*, 2311–2327.
[3] A. F. Wells, *Structural Inorganic Chemistry*, 5th ed., Oxford, New York, **1984**.
[4] a) K. A. Hirsch, D. Venkataraman, S. R. Wilson, J. S. Moore, S. Lee, *J. Chem. Soc. Chem. Commun.* **1995**, 2199–2200; b) D. Venkataraman, S. Lee, J. S. Moore, P. Zhang, K. A. Hirsch, G. B. Gardner, A. C. Covey, C. L. Prentice, *Chem. Mater.* **1996**, *8*, 2030–2040; c) O. Ermer, *J. Am. Chem. Soc.* **1988**, *110*, 3747–3754; d) O. Ermer, *Adv. Mater.* **1991**, *3*, 608–611; e) M. Simard, D. Su,

J. D. Wuest, *J. Am. Chem. Soc.* **1991**, *113*, 4696–4698; f) X. Wang, M. Simard, J. D. Wuest, *ibid.* **1994**, *116*, 12119–12120; g) B. F. Hoskins, R. Robson, *ibid.* **1990**, *112*, 1546–1554; h) L. R. MacGillivray, S. Subramanian, M. J. Zaworotko, *J. Chem. Soc. Chem. Commun.* **1994**, 1325–1326; i) L. Carlucci, G. Ciani, D. M. Proserpio, A. Sironi, *ibid.* **1994**, 2755–2756; j) M. Munakata, L. P. Wu, M. Yamamoto, T. Kuroda-Sowa, M. Maekawa, *J. Am. Chem. Soc.* **1996**, *118*, 3117–3124; k) A. Michaelides, V. Kiritsis, S. Skoulika, A. Aubry, *Angew. Chem.* **1993**, *105*, 1525–1526; *Angew. Chem. Int. Ed. Engl.* **1993**, *32*, 1495–1497; l) O. Ermer, L. Lindenberg, *Chem. Ber.* **1990**, *123*, 1111–1118; m) K. Sinzger, S. Hünig, M. Jopp, D. Bauer, W. Bietsch, J. U. von Schütz, H. C. Wolf, R. Kremer, T. Metzenthin, R. Bau, S. I. Khan, A. Lindbaum, C. L. Lengauer, E. Tillmanns, *J. Am. Chem. Soc.* **1993**, *115*, 7696–7705.

[5] From Figure 2b it is noted that the PF_6^- ions are significantly disordered. Thermogravimetric analysis and differential scanning calorimetry of crystals dried under vacuum overnight (to remove surface ethanol) shows a mass loss of approximately 5.5% at 95 °C, which corresponds approximately to two molecules of H_2O or one of ethanol in the unit cell. No molecules of ethanol or adventitious water could be located from the Fourier difference map.

[6] H. M. Powell, *J. Chem. Soc.* **1948**, 61–73.

[7] R. M. Hazen, L. W. Finger, *Comparative Crystal Chemistry*, Wiley, New York, **1982**.

[8] a) D. M. P. Mingos, A. L. Rohl, *Inorg. Chem.* **1991**, *30*, 3769–3771; b) D. M. P. Mingos, A. L. Rohl, *J. Chem. Soc. Dalton Trans.* **1991**, 3419–3425.

[9] The concept of interference in crystal engineering has been discussed qualitatively by Desiraju in the context of supramolecular synthons; see ref. [2b].

[10] J. S. Moore, unpublished results.

[11] M. Tashiro, T. Yamato, K. Kobayashi, T. Arimura, *J. Org. Chem.* **1987**, *52*, 3196–3199.